

# Robustness of topologically sensitive harmonic generation in laser-driven linear chains

Helena Drüeke and Dieter Bauer

*Institute of Physics, University of Rostock, 18051 Rostock, Germany*

(Dated: December 15, 2024)

A huge difference in the harmonic yield from the two topological phases of finite, dimerizing linear chains in laser fields has recently been observed in all-electron time-dependent density functional simulations [D. Bauer, K.K. Hansen, Phys. Rev. Lett. **120**, 177401 (2018)]. In this work, we explore the robustness of the effect concerning the size of the chains, a continuous transition between the two topological phases, and disorder. A high robustness of both the degeneracy of the edge states in the topologically non-trivial phase and of the pronounced destructive interference causing a dip in the harmonic spectra in the topologically trivial phase is observed.

## I. INTRODUCTION

The exploration of the territory between strong-field short-pulse laser and condensed matter physics has only recently gained momentum (see, e.g., [1–19]). One of the most fascinating research directions in condensed matter physics, cold atoms, and photonics are topological phases with interesting properties, and transitions between them [20]. From the strong-field laser perspective, there are only very few investigations on that subject to date [21–25]. Many questions arise in that context, for instance: How are topological phases encoded in typical strong-field observables such as photoelectron or harmonic spectra? How can strong, short-pulse lasers be used to manipulate topological phases? May topological edge states be useful to develop ultrafast, light-driven electronic devices or, *vice versa*, electronically driven, novel light sources? And from the theoretical perspective: Is the usual tight-binding modeling enough to properly describe the non-linear light-matter interaction? Which are the suitable and useful topological invariants? Does the laser need to illuminate the edges to have topological edge effects in photoelectron or harmonic spectra?

In Ref. [23], a many-order of magnitude different harmonic yield has been observed for the two topological phases of dimerizing linear chains that are well known from the Su-Schrieffer-Heeger (SSH) model [26, 27]. The huge difference in the harmonic yield was attributed to pronounced destructive interference of all the electrons' harmonic emission from the valence band of the topologically trivial phase A while the destructive interference is spoiled by the presence of half-occupied edge states in the topologically non-trivial phase B. This finding might, perhaps, be surprising because the modeling in Ref. [23] is based on time-dependent density functional theory (TDDFT) [28, 29], which goes far beyond the typical tight-binding, independent-electron treatment. In fact, it does so to an extent that the winding number, commonly considered as a topological invariant for the SSH model [27], does not apply to the TDDFT description. Nevertheless, the main topological feature of the SSH model—the presence of degenerate topological edge states—seems to be “inherited” by the TDDFT description without a winding number as a topological invariant.

From a practical point of view, robustness is the most appealing asset of topological matter because of potential applications in quantum computation (topological qubits [30]) or high-temperature superconductivity [31], for instance. In the current paper, we investigate the robustness of the huge topological effect in harmonic generation observed in [23] with respect to chain size, continuous phase transition, and disorder.

The paper is organized as follows: We review the TDDFT model in Section II. The robustness of the degeneracy of the edge states and the harmonic spectra is investigated in Section III as regards size dependence (subsection III A), continuous phase transition (subsection III B), and disorder in the ion positions and ion potentials (subsections III C and III D, respectively). We summarize in Section IV.

Throughout this paper, atomic units  $\hbar = |e| = m_e = 4\pi\epsilon_0 = 1$  are used unless stated otherwise.

## II. DENSITY-FUNCTIONAL MODEL FOR LINEAR CHAINS

The model system used in this work is the same as in [23], a linear chain of  $N$  singly charged ions. Starting from an equidistant spacing, the ions are alternately shifted by  $\delta$  to the left and to the right, leading to ion positions

$$x_i = \left(i - \frac{N+1}{2}\right)a - (-1)^i\delta, \quad i = 1, 2, \dots, N \quad (1)$$

with the lattice constant  $a$  and shift  $\delta$ . The interaction of an electron (at position  $x$ ) with the ions is described by the sum of the soft-core Coulomb potentials

$$v_{\text{ions}}(x) = \sum_{i=1}^N v_i(x) = - \sum_{i=1}^N \frac{1}{\sqrt{(x - x_i)^2 + \varepsilon_i}}. \quad (2)$$

We choose the same smoothing parameter for all ions,  $\varepsilon_i = 1$ , apart from subsection III D where topological robustness with respect to random fluctuations of the  $\varepsilon_i$  is investigated.

Time-dependent density functional theory [28, 29] is used to calculate the electronic states of the system and

its dynamics in the laser field. The time-dependent Kohn-Sham potential

$$v_{\text{KS}}[n](x, t) = v_{\text{ext}}(x, t) + u[n](x, t) + v_{\text{xc}}[n](x, t) \quad (3)$$

is the sum of the external potential  $v_{\text{ext}}(x, t)$ , the Hartree-potential  $u[n](x, t) = \int n(x', t)/\sqrt{(x-x')^2 + 1} dx'$ , where  $n(x, t)$  is the electron density, and the exchange-correlation potential  $v_{\text{xc}}[n]$ . The topological effects studied in the present work are robust with respect to the choice of  $v_{\text{xc}}[n]$  so that we use the simple adiabatic exchange-only local density approximation  $v_{\text{xc}}[n] \simeq -[3n(x, t)/\pi]^{1/3}$ . The external potential  $v_{\text{ext}}(x, t) = v_{\text{ions}}(x) - iA(t)\frac{\partial}{\partial x}$  consists of the ionic potential  $v_{\text{ions}}(x)$  and the coupling to the laser field described by the vector potential  $A(t)$  in velocity gauge and dipole approximation (with the  $A^2$ -term transformed away).

The implementation consists of two parts: First, imaginary-time propagation is used to self-consistently determine the occupied (and, if of interest, unoccupied) Kohn-Sham orbitals  $\varphi_i$  without external driver. In the second part, the influence of a laser pulse on the orbitals is simulated using real-time propagation. The orbitals are propagated according to the time-dependent Kohn-Sham equation

$$i\partial_t \varphi_i(x, t) = \left[ -\frac{1}{2} \frac{\partial^2}{\partial x^2} + v_{\text{KS}}[n](x, t) \right] \varphi_i(x, t) \quad (4)$$

with a split-operator Crank-Nicolson approximant [32]. For the real-time propagation with “unfrozen”  $u[n](x, t)$  and  $v_{\text{xc}}[n(x, t)]$ , the Kohn-Sham equation is nonlinear, and a predictor-corrector scheme is used. We restrict ourselves to spin-neutral systems in this work so that we suppress the spin index at the Kohn-Sham orbitals, and the total electron density reads  $n(x, t) = 2 \sum_{i=1}^{N/2} |\varphi_i(x, t)|^2$ .

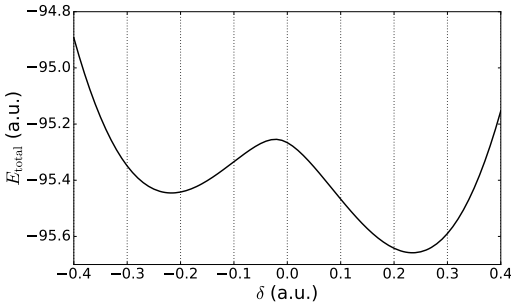


FIG. 1. Total energy for  $a = 2$  and  $N = 100$  vs shift  $\delta$ .

Figure 1 shows the total energy for the chain with lattice constant  $a = 2$  (throughout this paper) and  $N = 100$  singly charged ions as a function of the shift  $\delta$ . The total energy is calculated as  $E_{\text{total}} = E[\{\varphi_i\}] + E_{\text{ii}}$  with the static ion-ion energy  $E_{\text{ii}} = \sum_{i=1}^N \sum_{j < i} [(x_j - x_i)^2 + 1]^{-1/2}$  and the electronic energy  $E[\{\varphi_i\}] = T_s[\{\varphi_i\}] + E_{\text{ei}}[n] + U[n] + E_{\text{xc}}[n]$  where  $T_s[\{\varphi_i\}] = -\sum_{i=1}^{N/2} \int dx \varphi_i^*(x) \frac{\partial^2}{\partial x^2} \varphi_i(x)$  is the kinetic

energy,  $E_{\text{ei}}[n] = \int v_{\text{ions}}(x)n(x)dx$  is the electron-ion interaction energy,  $U[n] = \frac{1}{2} \int u[n](x)n(x)dx$  is the Hartree energy, and  $E_{\text{xc}}[n] \simeq -\frac{3}{4} (\frac{3}{\pi})^{1/3} \int n^{4/3}(x)dx$  is the exchange-correlation energy. There is a global minimum in the phase A ( $\delta > 0$ ) regime at  $\delta = 0.235$  and a local minimum in the phase B ( $\delta < 0$ ) at  $\delta = -0.217$  [33]. The metallic case  $\delta = 0$  is energetically unfavorable (Peierls instability).

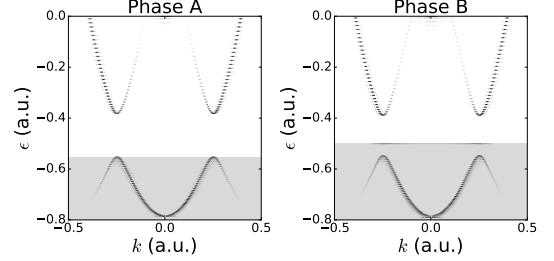


FIG. 2. Band structures of phases A ( $\delta = 0.235$ ) and B ( $\delta = -0.217$ ). The gray shades indicate the occupied electron orbitals.

Figure 2 shows the band structures of the two phases for the shifts  $\delta$  corresponding to the two local minima for  $N = 100$  in Fig. 1. We calculate band structures for finite chains by Fourier-transforming the position-space Kohn-Sham orbitals to  $k$ -space [34]. Phase A is an insulator with a completely filled valence band and an unoccupied conduction band. Two edge states are present in the band gap of phase B. They are degenerate and only one of them is occupied. In position space, these states are localized on the edges of the chain, hence the name.

The laser pulse used in this work is an  $n_{\text{cyc}} = 5$  cycle sine-square pulse of frequency  $\omega = 0.0075$  (which corresponds to a wavelength of  $\simeq 6.1 \mu\text{m}$ ). The vector potential reads

$$A(t) = A_0 \sin^2 \left( \frac{\omega t}{2n_{\text{cyc}}} \right) \sin \omega t \quad (5)$$

for  $0 < t < 2\pi n_{\text{cyc}}/\omega$  and zero otherwise. The dipole

$$X(t) = 2 \sum_{i=1}^{N/2} \int x |\varphi_i(x, t)|^2 dx \quad (6)$$

is recorded during the laser pulse. For some of the cases investigated in this work, the dipole  $X(0)$  before the interaction with the laser is not zero. To account for this,  $X(0)$  is subtracted, which only affects the harmonic component at frequency zero. The topological features in the harmonic spectra are qualitatively independent of whether we use the dipole, velocity, current or acceleration to compute the spectra [35, 36].

In order to improve the dynamic range of the harmonic spectra, the dipoles are windowed by a Hann function [37]  $w(t) = \sin^2 [\pi t / (N_t \Delta t - 1)]$ , where  $N_t$  is the number of outputs and  $\Delta t$  the output interval. The total dipole

strength  $D(\omega)$  is then calculated by taking the absolute square of the Fourier transform of the windowed dipole

$$D(\omega) \propto |\text{FFT}[w(t)X(t)]|^2. \quad (7)$$

### III. ROBUSTNESS OF TOPOLOGICAL EFFECTS ON HARMONIC GENERATION

In Ref. [23], a difference of up to 14 orders of magnitude between harmonic spectra for the two topological phases was found. The origin of this huge topological effect was attributed to the destructive interference of all the dipoles of the Kohn-Sham orbitals in phase A due to the completely filled valence band. Instead, for phase B destructive interference is imperfect because of the only half-occupied edge states. In the following, the remarkable robustness of that topological effect is illustrated.

#### A. Size dependence

The harmonic spectra for the two topological phases for  $N = 100$  ions and a vector potential amplitude  $A_0 = 0.1$  (i.e., an intensity of  $\simeq 2 \times 10^{10}$  W/cm<sup>2</sup>) are shown in Fig. 3. The huge difference in the harmonic yield observed already in [23] is clearly visible.

In order to investigate how many ions are needed to generate the characteristic spectra of the phases, the number of ions  $N$  is decreased. The effect of the chain length on the *high*-harmonic generation was investigated in Ref. [38], although not with a focus on topological effects. Here we are interested in the sub-band-gap regime (i.e., harmonic-photon energies are smaller than the band gap of phase A) where the huge *qualitative* difference in Fig. 3 is observed. The excursions of electrons and holes before recombination are obviously relevant for those interband harmonics generated by a three-step-like process [38, 39]. In the sub-band-gap regime, anharmonic intra-band motion of the electrons is the origin of harmonics, and its dependence on the chain length is not obvious. As the huge difference between phase A and B is an edge-state effect, one could expect that the ratio of surface (two ions in one dimension) to bulk (the other  $N - 2$  ions) is relevant while *topological* edge-state effects should be independent of  $N$  as long as  $N$  is big enough to yield an energy spectrum that resembles a band structure at all. Indeed, increasing  $N$  beyond 100 does not change qualitatively the harmonic spectra for both phases.

The harmonic spectra for  $N = 30$  are also shown in Fig. 3. Even though there are differences between the harmonic spectra for  $N = 100$  and  $N = 30$  ions in both phases, the huge difference in the sub-band-gap regime remains qualitatively the same.

Spectra for even smaller  $N$  were examined as well. Only when  $N$  is so small ( $N < 10$ ) that no band structure develops, the clear difference between the phases due

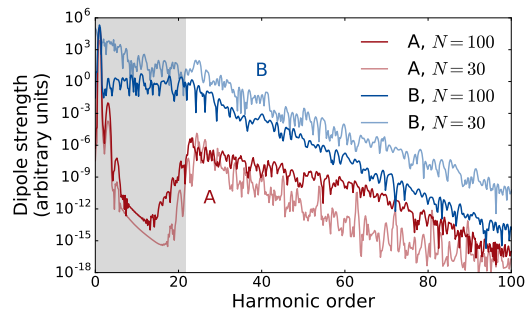


FIG. 3. Harmonic spectra of phases A and B for  $N = 100$  and  $N = 30$  ions. The gray shade indicates the sub-band-gap regime of phase A.

to perfect and imperfect destructive interference deteriorates. For the extreme case of  $N = 2$ , the two phases correspond to two diatomic molecules with by  $2\delta$  different internuclear distances where the notion of “edge states” does not make sense.

#### B. Transition between phases

Topological equivalence is often popularly explained as the possibility to continuously deform an object without pinching holes in it or breaking it. Topological difference thus implies the impossibility of such a deformation without changing the topological invariant (e.g., the number of holes in an object). In condensed matter physics the situation is a bit more complex, as the deformations can be continuous in position space but the topological invariant changes discontinuously in another, more abstract space. Topological invariants are typically defined for bulk material as winding numbers (e.g., in the space spanned by the  $2 \times 2$  matrices of a tight-binding Bloch hamiltonian as a function of lattice momentum  $k$ ), integrals over the Berry curvature in  $k$ -space, or simply the number of levels below some properly defined zero energy [27, 40, 41].

We can continuously go from phase B to phase A in position space by increasing the left edge ion’s coordinate  $x_1$  until it pairs up with the right edge ion to form a phase-A chain. Figure 4 shows the orbital energies during the transition for  $N = 100$  as well as the edge state orbitals for two exemplary configurations. For each configuration, the self-consistent, stationary electron structure is calculated (i.e., we are not moving the edge ion in real time but use  $x_1$  as an order parameter to describe a hypothetical, adiabatic phase transition).

One could expect that the degeneracy of the two edge-state energies is lifted as soon as the inversion symmetry is broken by an  $x_1 \neq -x_{100}$ . Instead, Fig. 4 shows that the edge-state levels remain degenerate until the edge-state orbitals start to overlap. For example, for  $x_1 \simeq 0$  (when the previously left-edge ion is moved to the center), the two contributions to the edge state orbitals from

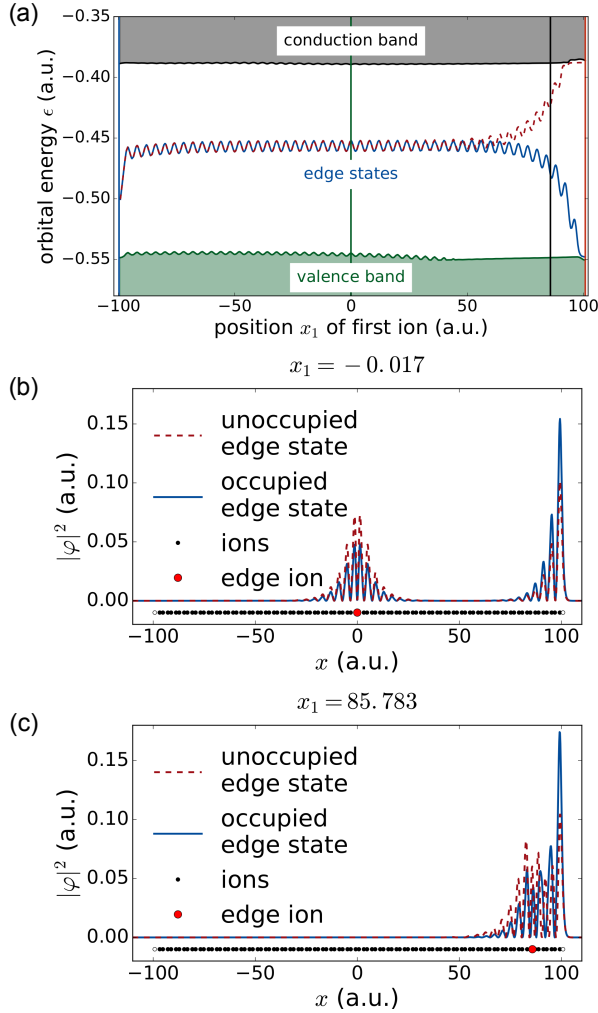


FIG. 4. (a) Orbital energies during the transition from phase B to phase A, (b) edge state orbitals for  $x_1 = -0.017$ , and (c)  $x_1 = 85.783$ .

the right edge and the shifted left-edge ion are still well separated. As a consequence, the energies of the two edge states are still degenerate, just slightly higher than in the original phase-B case. At  $x_1 \simeq 86$ , the edge states are not degenerate anymore because the contributions on the shifted ion and the right edge overlap significantly. The case  $x_1 = 100.783$  almost corresponds to the perfect phase-A case. One of the two degenerate edge states turned into the highest state of the valence band, the other one into the lowest of the conduction band.

Figure 5 shows harmonic spectra for several  $x_1$  during the transition, as indicated by vertical lines in Fig. 4(a). For  $x_1 = -0.017$  the harmonic spectrum is very similar to the pure phase-B case because the band structure did not change qualitatively (the two edge states are still degenerate). For  $x_1 = 85.783$ , the spectrum already shows a phase-A-like dip, although a smaller one and at lower harmonic order because the energy difference between the two now separated edge states is smaller than the band gap in pure phase A. At  $x_1 = 100.783$ , the spectrum looks

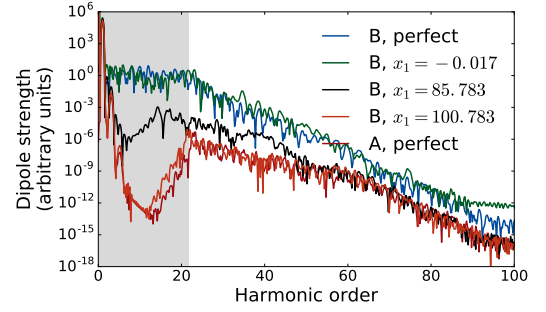


FIG. 5. Harmonic spectra for phase A, phase B, and phase B with  $x_1 = -0.017$ ,  $x_1 = 85.783$ , and  $x_1 = 100.783$ . The gray shade indicates the sub-band-gap regime of phase A.

almost like the one for pure phase A. Small deviations are due to the fact that phase B with  $x_1 = 100.783$  corresponds to phase A with  $\delta = 0.217$  instead of  $\delta = 0.235$  (where the total energy is minimal).

### C. Disorder in the ion positions

Topological systems with disorder are a topic of current scientific interest (see, e.g., [42, 43]). The role of disorder in harmonic generation has been investigated as well [13]. It has been found that disordered systems generate harmonics at least as well as ordered systems, showing that a band structure is not necessary for efficient harmonic emission from solids.

Disorder is introduced into our model system by randomly shifting the ion positions according to  $x_i \rightarrow x'_i = x_i + r_i$ , mimicking disordered samples or finite temperature. The random shifts  $r_i$  follow a normal distribution with mean 0 and standard deviation  $\sigma_x$ .

The harmonic spectra of phases A and B for different standard deviations  $\sigma_x$  and histograms of the internuclear distances are shown in Figure 6. In phase A, the characteristic low-harmonic yield below the band gap due to destructive interference of all the dipoles of Kohn-Sham electrons in the valence band disappears with increasing disorder. This is because the bands are “washed out” by disorder, which effectively decreases the band gap. However, the dip in the phase-A spectra survives up to surprisingly high  $\sigma_x = 0.4$  where the histogram of the internuclear distances does not show a two-peak distribution of a dimerized chain anymore.

The introduction of random shifts to the ion positions has little impact on the qualitative features of the harmonic spectrum from phase B. This is not surprising because there is no concerted destructive interference to be ruined by disorder in the first place. We hence show results only for extreme disorder  $\sigma_x = 1$  and  $\sigma_x = 2$ . For such high values, many of the random shifts are already on the order of the lattice constant  $a = 2$ , i.e., ions overtake each other. These spectra are thus examples for harmonic generation from purely random linear chains.

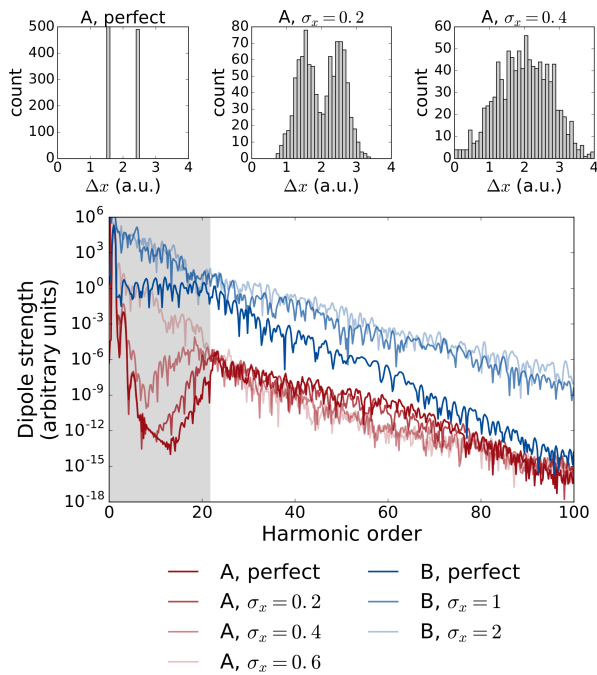


FIG. 6. Top: Histograms of the internuclear distances  $\Delta x$  for phase A with random shifts. Bottom: Harmonic spectra for phases A and B for different standard deviations  $\sigma_\varepsilon$ . The gray shade indicates the sub-band-gap regime of phase A.

#### D. Disorder in the ion potential

Another way to introduce disorder is to randomly vary the smoothing parameter  $\varepsilon_i$  in the Coulomb potentials  $v_i(x) = -[(x - x_i)^2 + \varepsilon_i]^{-1/2}$  of the ions, which affects the depth of the potential. One may view this as randomly changing the local ionization potentials of the atoms that constitute the chain. The  $\varepsilon_i$  follow a normal distribution with mean 1 and standard deviation  $\sigma_\varepsilon$ . If a random  $\varepsilon_i$  happens to be  $< 0$  it is set to 0.

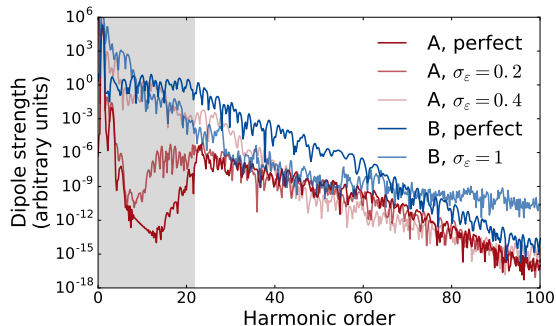


FIG. 7. Harmonic spectra of phases A and B for different standard deviations  $\sigma_\varepsilon$ . The gray shade indicates the sub-band-gap regime of phase A.

The harmonic spectra of phases A and B for different standard deviations  $\sigma_\varepsilon$  are shown in Figure 7.

In phase A, there are no large deviations in the above-band-gap regime (white background). Similar to the case of fluctuations of the ion positions in the previous subsection, in the sub-band-gap regime the characteristic low-harmonic yield disappears only for surprisingly large random variations.

#### IV. SUMMARY

Harmonic generation in different topological phases was investigated using a linear chain as a model system. The harmonic yield was calculated with time-dependent density functional theory, taking the response of all electrons to the laser field into account. The previously found low harmonic yield of phase A (without topological edge states) compared to phase B (with topological edge states) in the sub-band-gap regime was confirmed, and the robustness of this huge topological effect was studied with respect to (i) the size of the chain, (ii) a continuous transition between the two topological phases, and (iii) disorder. When the number of ions  $N$  in the system was lowered, both phases retained the characteristic features of their harmonic spectra down to very low  $N \simeq 10$ . During the continuous transition from phase B to phase A by moving one of the edge ions to the other side, the degeneracy of the edge states and the harmonic spectrum remained of phase-B character until the shifted ion paired up with the opposite edge ion. Random shifts of the ions and changes in the ionic potentials of the ions had to be surprisingly large to destroy the characteristic features of the harmonic spectra of both phases.

In view of possible applications, robustness is probably the most important and striking asset of topological effects. Hence one may argue that the observed robustness in the current paper is not surprising. However, it is important to point out that we observe this robustness for a time-dependent density-functional model of a strongly driven finite chain for which a winding number that could serve as a topological invariant (like for the Su-Schrieffer-Heeger model) does, to the best of our knowledge, not exist. Nevertheless, the essential feature of the Su-Schrieffer-Heeger model is inherited: the presence and robustness of degenerate edge states.

#### ACKNOWLEDGMENTS

Inspiring discussions with Alexander Szameit are gratefully acknowledged.

- [1] Shambhu Ghimire, Anthony D. DiChiara, Emily Sistrunk, Pierre Agostini, Louis F. DiMauro, and David A. Reis, “Observation of high-order harmonic generation in a bulk crystal,” *Nat Phys* **7**, 138–141 (2011).
- [2] Martin Schultze, Krupa Ramasesha, C.D. Pemmaraju, S.A. Sato, D. Whitmore, A. Gandman, James S. Prell, L. J. Borja, D. Prendergast, K. Yabana, Daniel M. Neumark, and Stephen R. Leone, “Attosecond band-gap dynamics in silicon,” *Science* **346**, 1348–1352 (2014).
- [3] O. Schubert, M. Hohenleutner, F. Langer, B. Urbanek, C. Lange, U. Huttner, D. Golde, T. Meier, M. Kira, S.W. Koch, and R. Huber, “Sub-cycle control of terahertz high-harmonic generation by dynamical Bloch oscillations,” *Nat Photon* **8**, 119–123 (2014), letter.
- [4] G. Vampa, T. J. Hammond, N. Thiré, B. E. Schmidt, F. Légaré, C. R. McDonald, T. Brabec, D. D. Klug, and P. B. Corkum, “All-optical reconstruction of crystal band structure,” *Phys. Rev. Lett.* **115**, 193603 (2015).
- [5] M. Hohenleutner, F. Langer, O. Schubert, M. Knorr, U. Huttner, S. W. Koch, M. Kira, and R. Huber, “Real-time observation of interfering crystal electrons in high-harmonic generation,” *Nature* **523**, 572–575 (2015), letter.
- [6] T. T. Luu, M. Garg, S. Yu Kruchinin, A. Moulet, M. Th Hassan, and E. Goulielmakis, “Extreme ultraviolet high-harmonic spectroscopy of solids,” *Nature* **521**, 498–502 (2015), letter.
- [7] M. Lucchini, S. A. Sato, A. Ludwig, J. Herrmann, M. Volkov, L. Kasmí, Y. Shinohara, K. Yabana, L. Gallmann, and U. Keller, “Attosecond dynamical Franz-Keldysh effect in polycrystalline diamond,” *Science* **353**, 916–919 (2016).
- [8] M. Th Hassan, T. T. Luu, A. Moulet, O. Raskazovskaya, P. Zhokhov, M. Garg, N. Karpowicz, A. M. Zheltikov, V. Pervak, F. Krausz, and E. Goulielmakis, “Optical attosecond pulses and tracking the nonlinear response of bound electrons,” *Nature* **530**, 66–70 (2016), letter.
- [9] Georges Ndashimiye, Shambhu Ghimire, Mengxi Wu, Dana A. Browne, Kenneth J. Schafer, Mette B. Gaarde, and David A. Reis, “Solid-state harmonics beyond the atomic limit,” *Nature* **534**, 520–523.
- [10] A. Sommer, E. M. Bothschafter, S. A. Sato, C. Jakubeit, T. Latka, O. Razskazovskaya, H. Fattahi, M. Jobst, W. Schweinberger, V. Shirvanyan, V. S. Yakovlev, R. Kienberger, K. Yabana, N. Karpowicz, M. Schultze, and F. Krausz, “Attosecond nonlinear polarization and light-matter energy transfer in solids,” *Nature* **534**, 86–90 (2016), letter.
- [11] F. Langer, M. Hohenleutner, U. Huttner, S.W. Koch, M. Kira, and R. Huber, “Symmetry-controlled temporal structure of high-harmonic carrier fields from a bulk crystal,” *Nat Photon* **11**, 227–231 (2017), letter.
- [12] Nicolas Tancogne-Dejean, Oliver D. Mücke, Franz X. Kärtner, and Angel Rubio, “Impact of the electronic band structure in high-harmonic generation spectra of solids,” *Phys. Rev. Lett.* **118**, 087403 (2017).
- [13] Yong Sing You, Yanchun Yin, Yi Wu, Andrew Chew, Xiaoming Ren, Fengjiang Zhuang, Shima Gholam-Mirzaei, Michael Chini, Zenghu Chang, and Shambhu Ghimire, “High-harmonic generation in amorphous solids,” *Nature Communications* **8**, 724.
- [14] Takuya Higuchi, Christian Heide, Konrad Ullmann, Heiko B. Weber, and Peter Hommelhoff, “Light-field-driven currents in graphene,” *Nature* **550**, 224 EP – (2017).
- [15] G. P. Zhang, M. S. Si, M. Murakami, Y. H. Bai, and Thomas F. George, “Generating high-order optical and spin harmonics from ferromagnetic monolayers,” *Nature Communications* **9**, 3031 (2018).
- [16] G. Vampa, T. J. Hammond, M. Taucer, Xiaoyan Ding, X. Ropagnol, T. Ozaki, S. Delprat, M. Chaker, N. Thiré, B. E. Schmidt, F. Légaré, D. D. Klug, A. Yu Naumov, D. M. Villeneuve, A. Staudte, and P. B. Corkum, “Strong-field optoelectronics in solids,” *Nature Photonics* **12**, 465–468 (2018).
- [17] Matthias Baudisch, Andrea Marini, Joel D. Cox, Tony Zhu, Francisco Silva, Stephan Teichmann, Mathieu Mascicotte, Frank Koppens, Leonid S. Levitov, F. Javier García de Abajo, and Jens Biegert, “Ultrafast nonlinear optical response of dirac fermions in graphene,” *Nature Communications* **9**, 1018 (2018).
- [18] M. Garg, H. Y. Kim, and E. Goulielmakis, “Ultimate waveform reproducibility of extreme-ultraviolet pulses by high-harmonic generation in quartz,” *Nature Photonics* **12**, 291–296 (2018).
- [19] Christian Heide, Takuya Higuchi, Heiko B. Weber, and Peter Hommelhoff, “Coherent electron trajectory control in graphene,” *Phys. Rev. Lett.* **121**, 207401 (2018).
- [20] Hui Zhai, Mikael Rechtsman, Yuan-Ming Lu, and Kun Yang, “Focus on topological physics: from condensed matter to cold atoms and optics,” *New Journal of Physics* **18**, 080201 (2016).
- [21] Hamed Koochaki Kelardeh, Vadym Apalkov, and Mark I. Stockman, “Graphene superlattices in strong circularly polarized fields: Chirality, Berry phase, and attosecond dynamics,” *Phys. Rev. B* **96**, 075409 (2017).
- [22] Tran Trung Luu and Hans Jakob Wörner, “Measurement of the Berry curvature of solids using high-harmonic spectroscopy,” *Nature Communications* **9**, 916 (2018).
- [23] Dieter Bauer and Kenneth K. Hansen, “High-harmonic generation in solids with and without topological edge states,” *Physical Review Letters* **120**, 10.1103/PhysRevLett.120.177401.
- [24] R. E. F. Silva, Jimnez-Galn, B. Amorim, O. Smirnova, and M. Ivanov, “Topological strong field physics on sub-laser cycle time scale,” *arXiv:1806.11232v2 [cond-mat, physics:physics]*.
- [25] Alexis Chacón, Wei Zhu, Shane P. Kelly, Alexandre Dauphin, Emilio Pisanty, Antonio Picón, Christopher Ticknor, Marcelo F. Ciappina, Avadh Saxena, and Maciej Lewenstein, “Observing topological phase transitions with high harmonic generation,” *arXiv:1807.01616 [cond-mat, physics:quant-ph]*.
- [26] W. P. Su, J. R. Schrieffer, and A. J. Heeger, “Solitons in polyacetylene,” *Phys. Rev. Lett.* **42**, 1698–1701 (1979).
- [27] J.K. Asbóth, L. Oroszlány, and A. Pályi, *A Short Course on Topological Insulators*, Lecture Notes in Physics, Vol. 919 (Springer, 2016).
- [28] Erich Runge and E. K. U. Gross, “Density-functional theory for time-dependent systems,” *Physical Review Letters* **52**, 997–1000.

- [29] C. A. Ullrich, *Time-Dependent Density-Functional Theory: Concepts and Applications* (Oxford University Press, Oxford, 2011).
- [30] Ady Stern and Netanel H. Lindner, “Topological quantum computation—from basic concepts to first experiments,” *Science* **339**, 1179–1184 (2013).
- [31] Valla Fatemi, Sanfeng Wu, Yuan Cao, Landry Bretheau, Quinn D. Gibson, Kenji Watanabe, Takashi Taniguchi, Robert J. Cava, and Pablo Jarillo-Herrero, “Electrically tunable low-density superconductivity in a monolayer topological insulator,” *Science* (2018), 10.1126/science.aar4642.
- [32] Dieter Bauer, ed., *Computational Strong-Field Quantum Dynamics* (DeGruyter, Berlin, 2017).
- [33] Figure 1 corrects panel (a) of Fig. 1 in [23] (which, however, does not affect any of the other results and the conclusions in [23]).
- [34] Kenneth K. Hansen, Tobias Deffge, and Dieter Bauer, “High-order harmonic generation in solid slabs beyond the single-active-electron approximation,” *Phys. Rev. A* **96**, 053418 (2017).
- [35] A. D. Bandrauk, S. Chelkowski, D. J. Diestler, J. Manz, and K.-J. Yuan, “Quantum simulation of high-order harmonic spectra of the hydrogen atom,” *Physical Review A* **79**, 023403.
- [36] Jan Conrad Baggesen and Lars Bojer Madsen, “On the dipole, velocity and acceleration forms in high-order harmonic generation from a single atom or molecule,” *Journal of Physics B: Atomic, Molecular and Optical Physics* **44**, 115601.
- [37] F. J. Harris, “On the use of windows for harmonic analysis with the discrete Fourier transform,” *Proceedings of the IEEE* **66**, 51–83 (1978).
- [38] Kenneth K. Hansen, Dieter Bauer, and Lars Bojer Madsen, “Finite-system effects on high-order harmonic generation: From atoms to solids,” *Phys. Rev. A* **97**, 043424 (2018).
- [39] G. Vampa and T. Brabec, “Merge of high harmonic generation from gases and solids and its implications for attosecond science,” *Journal of Physics B: Atomic, Molecular and Optical Physics* **50**, 083001 (2017).
- [40] M. Z. Hasan and C. L. Kane, “Colloquium,” *Rev. Mod. Phys.* **82**, 3045–3067 (2010).
- [41] Marcel Franz and Laurens Molenkamp, eds., *Topological Insulators*, Contemporary Concepts of Condensed Matter Science, Vol. 6 (Elsevier, 2013).
- [42] Cenke Xu and J. E. Moore, “Stability of the quantum spin hall effect: Effects of interactions, disorder, and  $\mathbb{Z}_2$  topology,” *Physical Review B* **73**, 045322.
- [43] Simon Stützer, Yonatan Plotnik, Yaakov Lumer, Paraj Titum, Netanel H. Lindner, Mordechai Segev, Mikael C. Rechtsman, and Alexander Szameit, “Photonic topological anderson insulators,” *Nature* **560**, 461–465 (2018).